Concerted Ion-Migration and Diffusion Induced Degradation in Lead-Free Ag_3BiI_6 Rudorffite Solar Cells under Ambient Conditions

Ashish Kulkarni,[1,2]* Feray Ünlü,[3] Namrata Pant,[4] Jagjit Kaur,[5,6] Christoph Bohr,[3] Ajay Kumar Jena,[1] Senol Öz,[1,7] Masatoshi Yanagida,[4,8] Yasuhiro Shirai,[8] Masashi Ikegami,[1] Kenjiro Miyano,[8] Yasuhiro Tachibana,[9] Sudip Chakraborty,[5,6] Sanjay Mathur,[3]* and Tsutomu Miyasaka[1]*

A.K. and F. Ü. Contributed equally to this work

[1]Graduate School of Engineering, Toin University of Yokohama, 1614, Kurogane Cho, Aoba, Yokohama, Kanagawa 225-8503, Japan.

[2](Present address) IEK5-Photovoltaics Forschungszentrum Jülich, 52425 Jülich, Germany.

[3]Department of Chemistry, Institute of Inorganic Chemistry, University of Cologne, Greinstrasse 6, 50939 Cologne, Germany.

[4]Integrated Graduate School of Medicine, Engineering and Agricultural Sciences, University of Yamanashi, 4 Chome-4-37 Takeda, Kofu 400-8510, Japan.

[5]Materials Theory for Energy Scavenging (MATES) Lab, Discipline of Physics, Indian Institute of Technology Indore, 453552, India.

[6](Present address) Materials Theory for Energy Scavenging (MATES) Lab, Harish-Chandra Research Institute (HRI) Allahabad, Chhatnag Road, Jhunsi, Allahabad 211019, India.

[7](Present address) Saule Technologies, and Saule Research Institute, Dunska 11, 54-427 Wroclaw, Poland.

[8]Centre for Green Research on Energy and Environmental Materials, National Institute for Materials Science (NIMS), 1-1 Namiki, Tsukuba, Ibaraki 305-0044, Japan.

[9]School of Engineering, RMIT University, Bundoora, Victoria 3083, Australia.

ABSTRACT

Silver bismuth iodide (SBI) materials have recently gained attention as non-toxic alternatives to lead perovskites. Although most of the studies have been focusing on photovoltaic performance, the inherent ionic nature of SBI materials, their diffusive behaviour, and influence on material/device stability is underexplored. Herein, $AgBi_2I_7$, Ag_2BiI_5, and Ag_3BiI_6 thin-films are developed in controlled ambient humidity conditions with a decent efficiency up to 2.32%. While exploring the device stability, it is found that Ag_3BiI_6 exhibits a unique ion-migration behaviour where Ag^+, Bi^{3+}, and I^- ions migrate and diffuse through the dopant-free hole-transport layer (HTL) leading to degradation. Interestingly, this ion-migration behaviour is relatively fast for the case of anti-solvent processed Ag_3BiI_6 thin-film-based devices contrasting the case of without anti-solvent and is not observed for other SBI materials-based devices. Theoretical calculations suggest that low decomposition enthalpy favours the decomposition of Ag_3BiI_6 to AgI and BiI_3 causing migration of ions to the electrode which is protected by employing thick HTL. The new mechanism reported herein underlines the importance of SBI material composition and fundamental mechanism understanding on the stability of Ag_3BiI_6 material for better solar cell design and also in extending the applications of unique ion-migration behaviour in various optoelectronics.

KEYWORDS: lead-free, silver bismuth iodide, ion-migration, gold electrode, degradation, solar cell, stability.

Graphical Abstract

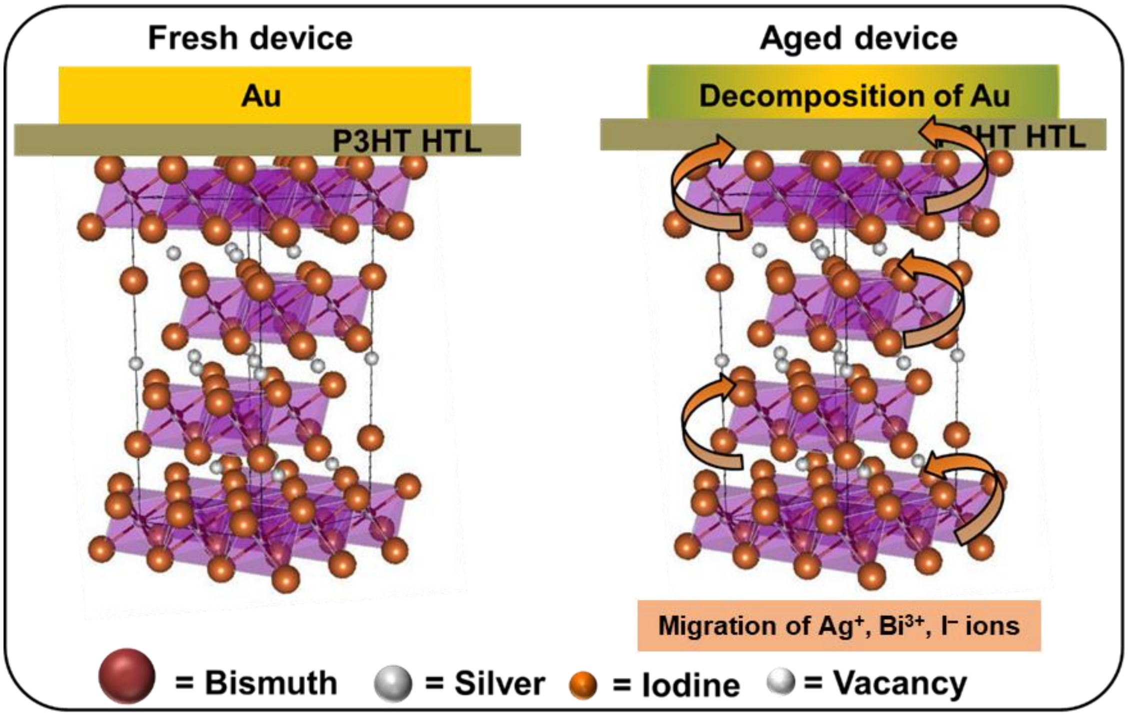

INTRODUCTION

Organic-inorganic hybrid lead-halide perovskite solar cells have witnessed a rapid rise in power conversion efficiency (PCE) from 3.8% to certified 25.5%.[1–3] Despite such advantages, perovskite degrades after exposure to moisture, heat, light, and oxygen.[4] In addition to this, intrinsic factors such as ion migration,[5] defects,[6] material instability,[7] nature of adjacent charge transport layers[8] also affect stability of the material. As a result, water-soluble ionic lead (Pb^{2+}) cation is released as an inherently toxic byproduct.[9] Development of lead-free perovskite, perovskite-inspired semiconducting materials with improved stability and efficiency is vital and is at the forefront of the research focus. Replacement of Pb^{2+} with tin (Sn^{2+}) was demonstrated first due to similar structural and electronic configurations. However, rapid oxidation of Sn^{2+} to Sn^{4+} under ambient atmosphere makes tin-perovskite even more unstable than their lead counterparts.[2,9,10] Due to its isoelectronic ($6s^2$) nature, efforts have been made to replace Pb^{2+} with bismuth (Bi^{3+}).[11] The assimilation of protonated cations such as methylammonium (MA^+) or cesium (Cs^+) into Bi–I octahedra forms Bi-based ternary halides ($A_3Bi_2I_9$; A = MA^+, Cs^+). These materials exhibit high absorption coefficients similar to lead perovskites and stability under ambient humidity atmosphere. Nevertheless, the photovoltaic device performance of $A_3Bi_2I_9$ absorber materials remained low mainly due to wide indirect band gap (E_g), high exciton binding energy, low electronic dimensionality induced anisotropic charge transport,[12,13] background carrier densities, and poor charge carrier mobility.[14,15]

Replacement of A-site cations (MA^+, Cs^+) with transition metals such as silver (Ag^+) or copper (Cu^+) results in the formation of a three dimensional (3D) edge-sharing octahedral network along with the reduction in optical band gap (from 2.3 eV for $A_3Bi_2I_9$ to <1.8 eV). Although these materials have been studied for several decades because of interesting optoelectronic properties and high ionic conductivity, their photovoltaic device performance has been realized lately. Initially, Sargent and coworkers have employed $AgBi_2I_7$ as an absorber material and reported a PCE of 1.22%.[16] Recently, we tuned the crystallization of $AgBi_2I_7$ by employing a weak solvent-intermediate adduct and reported PCE of 2.3% with high stability and reproducibility.[17] The photovoltaic device with hexagonal Ag_2BiI_5 absorber, as demonstrated by Johansson and coworkers, showed PCE of 2.1% in mesoscopic device architecture.[18] Turkevych et al. employed Ag_3BiI_6 light absorber in mesoscopic architecture and the device with poly[bis(4-phenyl)(2,4,6-trimethylphenyl)amine (PTAA) hole transport layer (HTL) showed PCE of 4.3%.[19] Recently, Pai et al. employed argon (Ar) gas quenching during the spin-coating step to obtain Ag_3BiI_6 film and achieved a PCE of 4.38% and 2.69% with PTAA and poly-3-hexylthiophene-2,5-diyl (P3HT) HTL respectively.[20] Dynamic casting with ramp annealing step, as demonstrated by Seo and co-workers, improved the morphology, and the inverted planar Ag_3BiI_6 device with nickel oxide (NiO_x) HTL showed a PCE of 1%.[21] Although these studies[19–22] have demonstrated decent initial efficiency and stability over hybrid lead perovskites, the inherent ionic nature of silver bismuth iodide (SBI) materials raises analogous ion migration concerns that effects device long-term stability.

Ion migration in hybrid lead halide perovskite has been rigorously studied and is revealed to be a contributing factor for ferroelectricity,[23] hysteresis behavior in the device current-voltage characteristic curve,[24] and device operational stability.[25] Due to the low activation energy, halide anions, and A-site cations in ABX_3 perovskite crystal structure ($A = MA^+$, Cs^+; $B = Pb^{2+}$; $X = I^-$, Cl^-, Br^-) are found to be the migrating species, while the metal (Pb^{2+}) cation tends to be immobile.[26] On the other hand, to the best of our knowledge, very little is known about the ion migration in SBI materials. Oldag et al. reported the activation energy of Ag^+ cations migration to be 0.4 eV in the Ag_3BiI_6 single crystal which is similar to the activation energy of iodine migration (0.44 eV) in lead-halide perovskites.[27] However, experimental evidence on the ion-migration[28,29] of Ag_3BiI_6 material and its dependence on the thin-film deposition method remains rare, such as the mobile species, their diffusive behaviors, and their influence on material/device stability. Herein, we report a unique ion-migration behavior of Ag_3BiI_6 solar cells employing dopant-free P3HT HTL. Contrasting the predominant role of halide in ion-migration in widely studied lead halide perovskites, we found that Ag_3BiI_6 based devices adopt a unique triple-ion-migration induced degradation, where Ag^+, Bi^{3+}, and I^- migration and diffusion occurs in the long-term operation of the devices. This migration is also dependent on the thin-film deposition method and on compositions of the SBI material and only occurs in the Ag-rich phase material. From theoretical studies, we observed that the decomposition reaction of Ag_3BiI_6 into silver iodide (AgI) and bismuth iodide (BiI_3) is exothermic and hence thermodynamically favored, which can be the main reason for the migration of ions. This migration of ions to the gold electrode can be protected by using thick HTL and also by employing the suitable SBI composition containing less amount of Ag-rich phase to fabricate solar cells.

RESULTS AND DISCUSSION

SBI thin films were obtained by dissolving 50 wt. % each of AgI and BiI_3 in a stoichiometric ratio in dimethylsulfoxide (DMSO) followed by spin coating the solution on TiO_2 mesoporous layer coated FTO substrates and annealing at 85 °C for 5 min and at 100 °C for 20 min. For the anti-solvent dripping, 1 mL of chlorobenzene (CB) was dropped over the substrate during the spin coating step as shown in **Figure S1** and outlined in the experimental section in the electronic supplementary information (ESI). **Figure 1a** shows the schematic illustration of the device architecture employing $AgBi_2I_7$, Ag_2BiI_5, and Ag_3BiI_6 materials. It is important to note that we employed a hot-casting method to obtain SBI ($AgBi_2I_7$, Ag_2BiI_5, and Ag_3BiI_6) thin-films because the process has been previously reported to improve device performance.[19] The formation of different SBI materials deposited *via* the anti-solvent method was monitored using X-ray diffraction (XRD) measurements and the results are in agreement with the previous reports.[16,18,19] **Figure S2** compares the literature diffraction data with the experimental one showing the peak positions and relative intensities. In addition to the XRD signatures of SBI materials, additional peaks were observed in the XRD patterns (marked with * in **Figure 1b**) assigning to AgI. This indicates the presence of residual or unreacted AgI in the SBI films. The residual AgI peak intensity increases with an increase in the AgI content in the SBI material showing the order of $Ag_3BiI_6 > Ag_2BiI_5 > AgBi_2I_7$ as shown in **Figure 1b** and **Figure S3**. Koedtruad et al. reported that for several compositions of Ag-Bi-I materials in particular Ag_3BiI_6 and Ag_2BiI_5, the related phases and AgI co-exist at room temperature, which we observed in our study.[30] In the case of the Ag-deficient composition $AgBi_2I_7$, the obtained XRD pattern is consistent with the previous report by Mashadieva et al.[31] additionally with a doublet peak at 42°. Previously, we reported that this doublet peak is due to remnant BiI_3 which additionally plays an important role in enhancing the performance and stability of $AgBi_2I_7$ solar cells.[17] The difference in the peak intensity of residual AgI in Ag_3BiI_6 compared to previous reports[19,20,32] might be due to the fabrication of thin-film in an ambient atmosphere with controlled humidity and the use of DMSO solvent (please see the experimental section for more details). Cross-sectional SEM micrographs of $AgBi_2I_7$ (**Figure 1c)** and Ag_2BiI_5 (**Figure 1d)** showed uniform interface with adjacent charge transport layers whereas, in the case of Ag_3BiI_6, a large number of voids were observed (**Figure 1e**) near the TiO_2 interface. Another cross-sectional SEM image of the Ag_3BiI_6 device showing voids over a large area is shown in **Figure S4**. Different crystallization process on the surface and at Ag_3BiI_6/TiO_2 interface (as illustrated in **Figure S5** and explained in **Explanation E1** in ESI) is suspected to be the reason for the formation of voids. In addition to this, bright dots were observed in all the cases, as shown in cross-sectional SEM images (**Figure 1c, 1d, and 1e**), which can be attributed to aggregates of the Ag-rich phase.[33,34] Previously, Bekenstein et al. also observed the formation of the Ag-rich phase in $Cs_2AgBiBr_6$ nanocrystals due to the less-standard reduction potential of silver.[33] Interestingly, in the case of $AgBi_2I_7$ and Ag_2BiI_5, bright dots were observed only on the surface of the TiO_2 mesoporous layer whereas in the Ag_3BiI_6 case, they were observed on the surface of Ag_3BiI_6 and Au metal electrode as shown in **Figure 1c**, **Figure 1d,** and **Figure 1e** respectively. Another cross-sectional SEM image of the Ag_3BiI_6 device showing accumulation of white dots (Ag-rich phase) on the surface of the Au metal electrode is shown in **Figure S6**. The presence of voids at the bottom interface (**Figure 1e, Figure S4**) and bright dots on the surface of the Ag_3BiI_6 layer and Au metal electrode (**Figure 1e, Figure S6**) indicates the more accumulation of AgI (Ag-rich phase) near the Ag_3BiI_6/P3HT/Au interface. Moreover, the presence of voids and non-uniform interfacial connection indicates that the Ag_3BiI_6 device undergoes high internal resistance and/or large recombination and improper interfacial charge transfer and might result in low device efficiency compared to $AgBi_2I_7$ and Ag_2BiI_5. As expected, the current density (J)-voltage (V) characteristic curves of the best performing photovoltaic device, as shown in **Figure 1f**, incorporating $AgBi_2I_7$, Ag_2BiI_5 and Ag_3BiI_6 absorber with P3HT HTL showed PCE of 2.1, 2.04, and 1.8% respectively. The photovoltaic device parameters of best-performing device J-V curves and statistics showing the reproducibility of the device performance are tabulated in **Table S1** and **Figure S7** respectively. While exploring the device stability in ambient humidity (RH = 30 – 50 %) atmosphere, it was interesting to observe that $AgBi_2I_7$ and Ag_2BiI_5 devices showed stable efficiency for ~12 weeks whereas Ag_3BiI_6 device performance started degrading within 2 weeks as shown in **Figure 1e**. This degradation was accompanied by the visual change in the color of the Au metal electrode which turned from yellow to greenish-yellow as shown in **Figure S8**. This was also observed by Crovetto et al., who suspected that ion migration causes the degradation,[35] however the AgI impurity and its effects on the device degradation were not investigated.

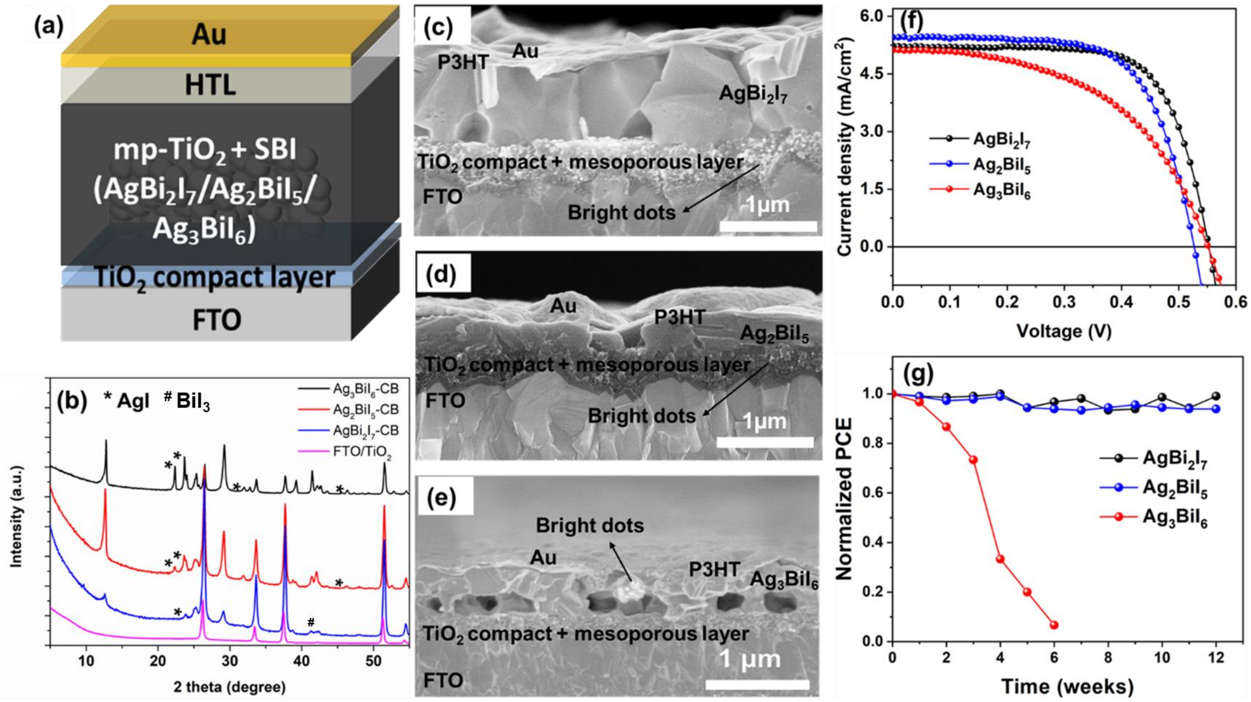

Figure 1: Comparison of SBI material properties and photovoltaic performance a) n-i-p mesostructured device architecture; b) XRD patterns obtained from thin-films of Ag_3BiI_6 (black), Ag_2BiI_5 (red) and $AgBi_2I_7$ (blue) on FTO/TiO_2 substrate (magenta); c-e) cross-section SEM images of the SBI solar cell devices processed with anti-solvent; f) J-V curves of best performing SBI solar cells and g) stability of the best performing SBI solar cells over several weeks.

The device performance degradation of the Ag_3BiI_6 device was suspected to be due to (1) the presence of a high amount of residual AgI near the surface and/or (2) due to the voids at the interface of TiO_2. This further indicates that a void-free layer might help in enhancing stability. Therefore, to investigate this, we obtained void-free Ag_3BiI_6 thin-film by depositing it without anti-solvent and compared it with the Ag_3BiI_6 device processed with anti-solvent dripping. The XRD pattern of Ag_3BiI_6 with and without voids, as shown in **Figure 2a** and **Figure S2c**, showed an insignificant difference.[19,20] However, the XRD pattern of Ag_3BiI_6 thin-film processed with anti-solvent (**Figure 2a**) showed higher peak intensity compared to without anti-solvent case evidencing improved crystallinity. Residual AgI was also observed in the XRD pattern of the without anti-solvent processed Ag_3BiI_6 thin-film as shown in **Figure S2c**. The ratio of XRD peak intensities of AgI and Ag_3BiI_6 with respect to highest peak intensity oriented along (003) crystal plane, as shown in **Figure S9**, clearly indicates the insignificant difference in the amount of residual AgI in without and with anti-solvent processed Ag_3BiI_6 thin-films. The non-existence of Ag_3BiI_6 in a pure single phase at room temperature can be the reason for the residual AgI content.[19] The unreacted or residual AgI might also lead to unreacted/residual BiI_3, however, the residual BiI_3 peaks were not detected in the XRD pattern most probably due to the overlapping of some of the BiI_3 and Ag_3BiI_6 XRD peaks as shown in **Figure S10**. In contrast to the anti-solvent-based Ag_3BiI_6 case, without anti-solvent-based Ag_3BiI_6 device showed bright dots primarily near the mesoporous TiO_2 layer (**Figure 2b**) with no voids. Another cross-sectional SEM image showing bright dots near the TiO_2 interface and void-free layer is shown in **Figure S11**. The difference in the location of bright dots can further be corroborated from top surface SEM images. **Figure 2c** shows a small amount of bright dots on the surface of Ag_3BiI_6 grains that was processed without the anti-solvent dripping step. On the other hand, these dots were observed in a higher amount near the grain boundaries for the anti-solvent case as shown in **Figure 2d**. This further suggests the presence of a higher amount of residual AgI on the surface of Ag_3BiI_6 grains and at the Ag_3BiI_6/P3HT/Au interface. Furthermore, Ag_3BiI_6 grains showed circular morphology in both the cases with a slightly flat surface for with anti-solvent based film as shown in **Figure 2c** and

Figure 2d, respectively. The difference in the morphology compared to previous reports[20,32] is mostly due to the choice of solvent and thin-film processing conditions. True non-contact atomic force microscope (AFM) measurements (**Figure S12b**) substantiated low root mean square (RMS) roughness of 15 nm and improved surface uniformity for Ag_3BiI_6 film processed with anti-solvent dripping in comparison to without anti-solvent case (**Figure S12a**) which showed RMS roughness of 70 nm and is line with top surface SEM morphology.

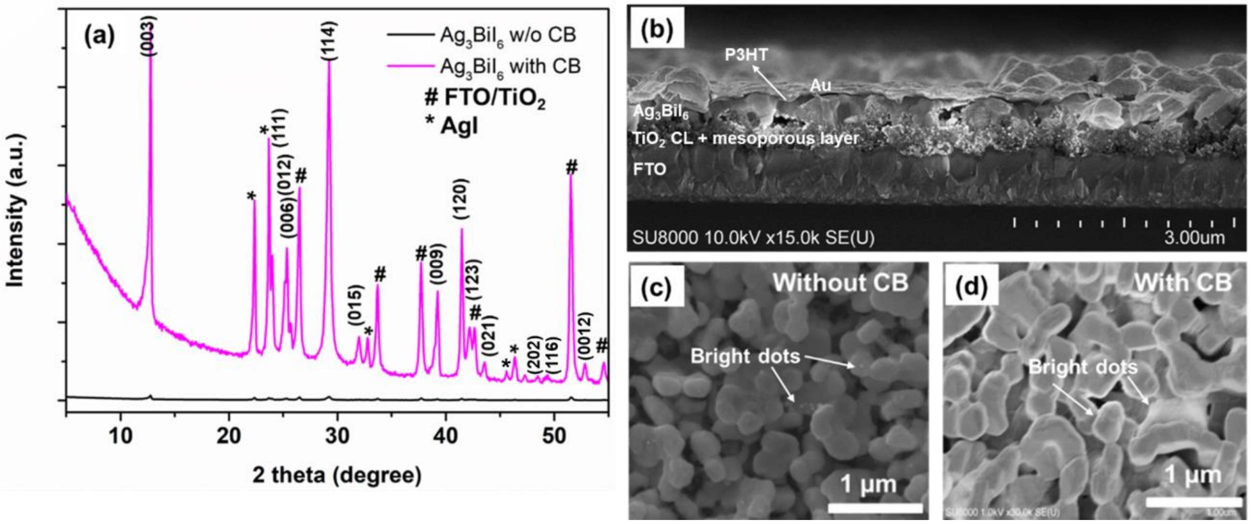

Figure 2: a) XRD pattern of Ag_3BiI_6 thin-film processed with and without anti-solvent, the peaks were indexed according to the data from Oldag et al.[27]; b) cross-section SEM image of Ag_3BiI_6 solar cell processed without anti-solvent method; top view SEM images of Ag_3BiI_6 thin-film c) without and d) with anti-solvent dripping.

Photophysical properties of Ag_3BiI_6 films processed without and with anti-solvent were investigated by steady-state photoluminescence (PL). This investigation helps to gain insights into the effect of anti-solvent dripping and residual AgI on the charge carrier recombination in Ag_3BiI_6 film. A broad PL peak was observed, as shown in **Figure S13a**, which is consistent with the previous report.[19] Moreover, PL analysis showed a higher peak intensity for anti-solvent-based Ag_3BiI_6 film compared to without anti-solvent one. A blue shift in the PL peak (**Figure S13b**) was correspondingly observed for Ag_3BiI_6 film processed with anti-solvent. The exact reason for the enhanced PL peak intensity and blue shift is not known at the moment but it might be due to low trap/defect sites and recombination centers[36,37] in the bulk of Ag_3BiI_6 and/or could also be within the experimental error mostly because of the existence of impure phase or multiphase features. Besides this, the PL showed a small additional peak at around ~735 nm which can be ascribed to the Ag_3BiI_6 impure phase (presence of residual AgI) and/or multiphase features.[19,20,32]

Photovoltaic characteristics were studied to elucidate the effect of a void-free layer on efficiency and stability. From the *J–V* characteristic curves (**Figure 3a**) of the best performing device and the box plots (**Figure S14**), it is evident that Ag_3BiI_6 devices processed without anti-solvent dripping showed better photovoltaic performance (best device showed PCE of 2.3%) in comparison to anti-solvent based Ag_3BiI_6 devices (best device showed PCE of 1.8%). The obtained efficiency (for without anti-solvent case) is among the best in the same category of Ag_3BiI_6 solar cells employing dopant-free P3HT as HTL.[20] The anti-solvent processed device showed large hysteresis in the device J-V curve compared to without anti-solvent one as shown in **Figure S15a**. The IPCE spectra of the best performing device and the photovoltaic device parameters are shown and tabulated in **Figure S15b** and **Table S2**, respectively. Despite showing enhanced PL peak intensity, the presence of voids, and a non-uniform interface in anti-solvent-based Ag_3BiI_6 devices attributes to low efficiency. On exposure to ambient atmosphere (humidity = 30 – 50%), without anti-solvent based Ag_3BiI_6 device degraded slowly (after 15 weeks) as compared to with anti-solvent one (after 1 week) as shown in **Figure 3b**. The performance degradation was additionally accompanied by a visual change in the color of the Au metal electrode, as shown in **Figure 3c**, evidencing its degradation. It is important to note that for without anti-solvent case, the visual color of Au changed after several weeks whereas in the case of anti-solvent based Ag_3BiI_6 device the

Au decomposed in two weeks, and prolonged exposure to ambient atmosphere resulted in a complete change in the color of the substrate (**Figure 3c**) indicating complete device failure.

To understand the Ag_3BiI_6 device degradation in the presence of other other dopant-free HTL we employed a dopant-free conjugated copolymer Poly[(dithieno[3,2-b:2′,3′-d]silolethieno[3,4-c]pyrrole-4,6-dione)-random-(2,2′-bithiophenethieno[3,4-c]pyrrole-4,6 dione)] (poly(DTSTPD-*r*-BThTPD)) HTL. The structure of the (poly(DTSTPD-*r*-BThTPD)) HTL is shown in **Figure S16a**. This HTL was previously synthesized and employed by our group in all-inorganic-based lead perovskite solar cells showing high V_{OC}.[7,38] When the same HTL was employed, the Ag_3BiI_6 device showed slight enhancement in the V_{OC} compared to the P3HT HTL (**Figure S16b**). However, the Au deposited on poly(DTSTPD-*r*-BThTPD) HTL decomposed in two weeks similar to that of the P3HT case (**Figure S16c**) clearly indicating that the Ag_3BiI_6 device degradation is independent of the HTLs employed. To understand the sensitivity of Ag_3BiI_6 thin-film under ambient humidity conditions, we intentionally stored anti-solvent processed Ag_3BiI_6 film in ambient conditions for two weeks followed by deposition of P3HT and Au and compared their structural, morphological, and photovoltaic performance with the ones that were freshly prepared. As can be seen in **Figure S17** and **Figure S18**, the UV-vis absorption spectra, XRD pattern, surface morphology, and the performance of the device made of Ag_3BiI_6 films which were intensionally stored for two weeks showed insignificant difference compared to that of freshly prepared Ag_3BiI_6 thin-film and devices. The UV-vis spectrum of fresh Ag_3BiI_6 thin film is shown in **Figure S23** and details will be discussed later. Interestingly, the performance of a device made of aged Ag_3BiI_6 thin-film degraded only after depositing the P3HT and Au electrode and the degradation trend was similar to that of the device obtained from freshly prepared Ag_3BiI_6 device as shown in **Figure S18b**. This degradation can be possibly related to the internal electric fielddriven migration and diffusion of ions towards the Au electrode which is corroborated by large hysteresis in the device J-V curve (**Figure S15a**) for the anti-solvent based device suggesting a high amount of ion-migration and faster degradation compared to without anti-solvent case. According to a previous report, part of silver which is localized in the Ag_3BiI_6 crystal structure varies with temperature and moves within the crystal structure.[27] From this, it can be envisaged that the residual AgI that is observed in Ag_3BiI_6 thin-film causes migration through thin P3HT HTL to corrode the Au electrode and degrade the performance as both Ag^+ and I^- are highly mobile due to low activation energy. Moreover, fast degradation in the anti-solvent case indicates that the voids at the TiO_2/Ag_3BiI_6 interface and accumulation of residual AgI on the surface can cause migration and diffusion of ions at a faster rate. It is important to note that devices were stored in an ambient atmosphere in the presence of light and to verify the migration of ions in the presence of light, the anti-solvent processed Ag_3BiI_6 device was exposed to 1 Sun (100 mW/cm^2) continuous illumination held at maximum power point tracking (MPPT). As can be seen from **Figure S19**, the Ag_3BiI_6 device containing voids and Ag-rich phase near the Ag_3BiI_6/P3HT/Au interface showed slow but linear degradation, however, it maintained PCE up to ~1.5% (initial efficiency = 1.8%) after 5000 s indicating that light illumination (in addition to ambient atmosphere) might cause ion-migration and performance degradation. The decomposition of AgI via photochemical reaction[39] hints towards the linear and slow degradation of the performance under continuous light illumination.

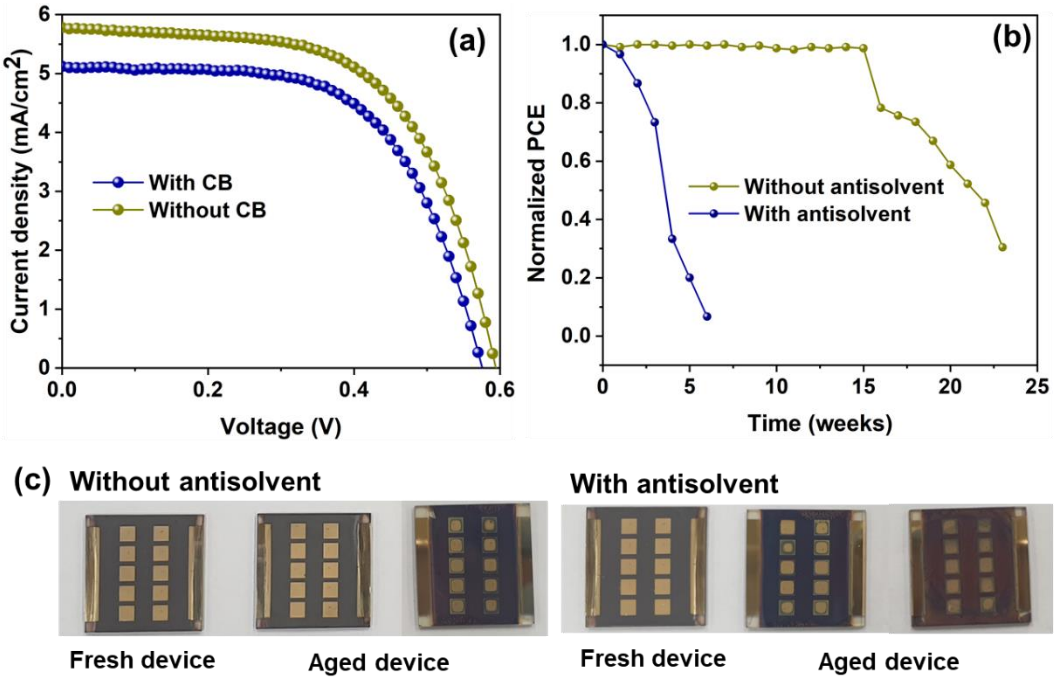

Figure 3: Performance and stability of Ag_3BiI_6 solar cells fabricated with and without the anti-solvent method a) J-V curves of best performing solar cells of thin-films with and without anti-solvent; b) Stability of the PCE over several weeks and c) Photographs of fresh and aged Ag_3BiI_6 solar cell devices showing slow and fast degradation for without and with anti-solvent case.

To confirm the migration of Ag^+ and I^- ions and their role in performance deterioration, X-ray photoelectron spectroscopy (XPS) was performed on the aged device showing both yellow (non-degraded region) and green (degraded region) areas of Au, and the results are shown in **Figure 4**. The XPS peaks on the yellow part of the Au (**Figure 4a inset**) appeared at 84.2 eV and 87.8 eV belonging to the $4f_{7/2}$ and $4f_{5/2}$ orbitals, respectively, as shown in **Figure 4a**. These values belong to the metallic form of Au which appears at 84 eV and 88 eV.[40,41] These 4f XPS peaks, on the degraded part of Au (**Figure 4b inset**), showed a shift from metallic (84.2 eV and 87.8 eV) to higher binding energy (84.9 eV and 88.6 eV) evidencing oxidation of Au^0 to Au^{+1}.[42] Moreover, a small peak corresponding to Au^{+3} was also observed at around 86 eV as shown in **Figure 4b**.[41] In addition to this, a relatively large amount of iodine ($3d_{5/2}$ peak) was detected (**Figure 4c and Figure 4d**) on the surface of the Au. The migration of residual AgI to the Au electrode top surface can be the source of iodine because Ag *3d* peak was detected on the surface of Au as shown in **Figure 4e** and **Figure 4f**. The presence of Ag^+ and I^- corroborates the cross-sectional SEM image (**Figure S6**) showing bright dots on the surface of the Au. We observed Ag 3*d* peak at 368.17 eV on the yellow area (non-degraded region) and at 368.3 eV on the green area (degraded region) assigning to Ag^+ (AgI) and Ag^0 respectively.[43] This peak shift from lower binding energy to higher binding energy indicates the reduction of AgI to Ag metallic. Another image showing a slight shift in the peak position of Ag is shown in **Figure S20**. Besides this, it was surprising to observe the presence of bismuth (Bi^{3+}) on the surface of the Au top electrode. Although Bi^{3+} has a large ionic radius and high ion migration energy barrier (3.363 eV), we suspect that the presence of voids might have facilitated the migration of Bi^{3+}. In the yellow area of Au, high intense and low intense Bi 4*f* peaks[40] (**Figure 4g**) appeared corresponding to Bi^{3+} and Bi^0, respectively.[44] According to previous reports, BiI_3 possesses a lot of interstitial defects, where bismuth is not bonded to iodine atoms.[45,46] This might be the reason for the appearance of the Bi^0 peak in the XPS spectra. There could also be a possibility arising from impurities or admixtures leading to the presence of metallic bismuth. Interestingly, the intensity of the Bi^0 metallic peak at 157 eV becomes intense in the green region (degraded part) of the Au (**Figure 4h**) indicating reduction of the higher amount of Bi^{3+} to metallic Bi^0 and removal of iodide. Chemical shifts of Au cannot be clearly explained by the physisorption of AgI or BiI_3 or I_2 on the surface of electrodes. Instead, the oxidation of Au^0 to Au^{+1} and Au^{+3}, presence of iodine, and reduction of Ag^+ to Ag^0 and Bi^{3+} to Bi^0 indicate that Au has reacted with iodine leading to degradation of the cell.

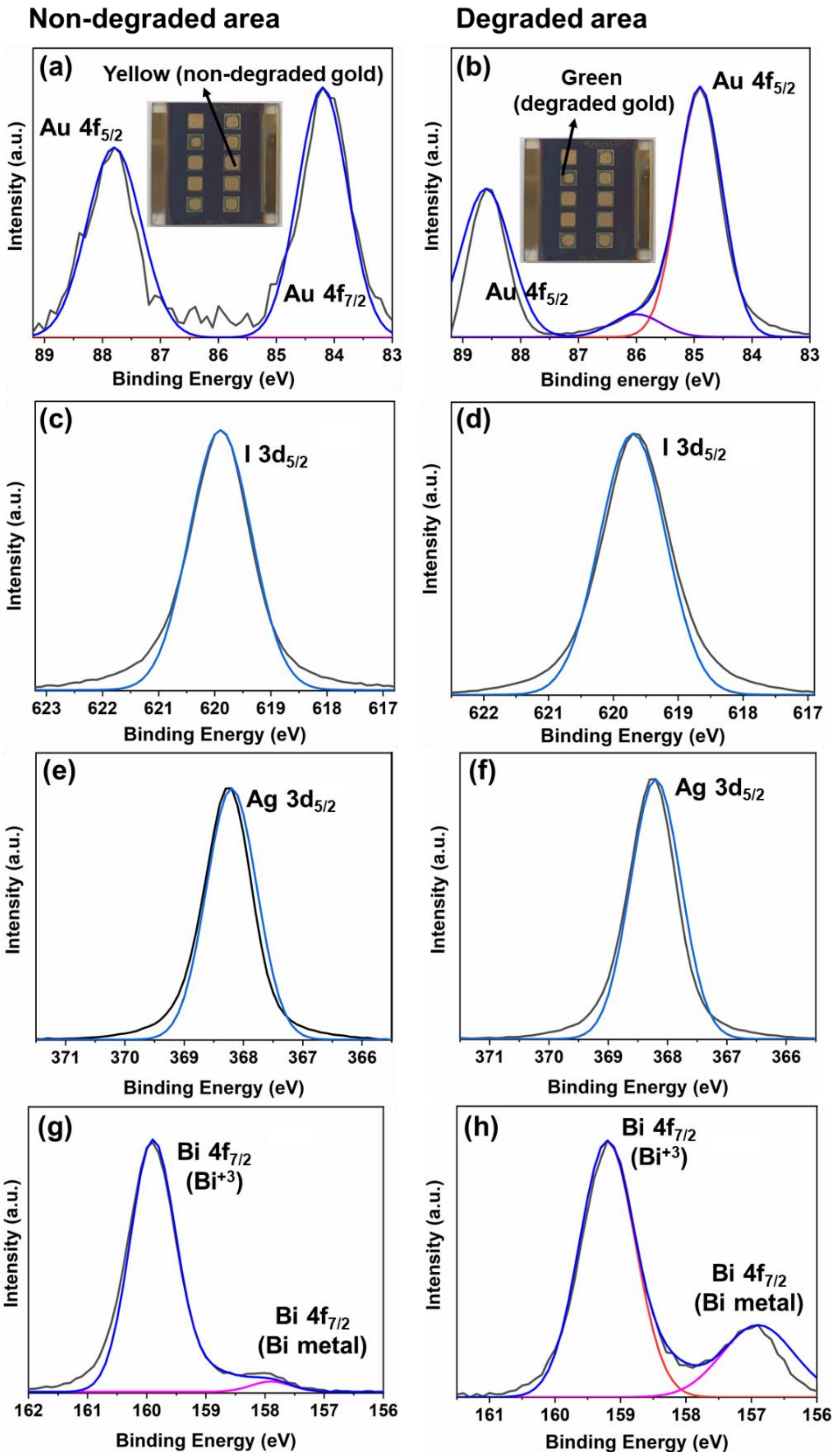

Figure 4: XPS core level spectra of a)-b) gold 4f; c)-d) iodine 3d; e)-f) silver 3d; g)-h) bismuth 4f of non-degraded electrode area and degraded electrode area, respectively.

To understand the triple-ion-migration and phase separation of BiI_3 and AgI, we have performed first-principles electronic structure calculations within the density functional theory (DFT) framework to provide additional insight from the perspective of electronic and optical properties of the material (detailed DFT simulations can be found in Explanation E2 in the supporting information). From the total DOS (**Figure S22**), calculated by Hybrid functional (HSE06) considering the spin-orbit coupling of the heavy metal Bi, we observed a band gap of 1.8 eV, which agrees with our experimental results (UV-vis spectra of Ag_3BiI_6 thin-film and its corresponding Tauc plot is shown in **Figure S23**). With the help of our total energy calculations based on the DFT formalism, we determined the decomposition enthalpy of the possible degradation pathway of Ag_3BiI_6. The decomposition enthalpy is calculated specifically for the degradation pathway: $Ag_3BiI_6 \xrightarrow{\Delta H} 3AgI + BiI_3$, where the minimum energy configuration of the individual bulk system has been achieved through complete ionic relaxation. The corresponding decomposition enthalpy (ΔH) was found to be –0.053 eV per formula unit, where the negative sign signifies the favorable degradation to occur as an exothermic reaction. This resembles well with the experimental result, where the degradation of Ag_3BiI_6 to AgI and BiI_3 is observed.

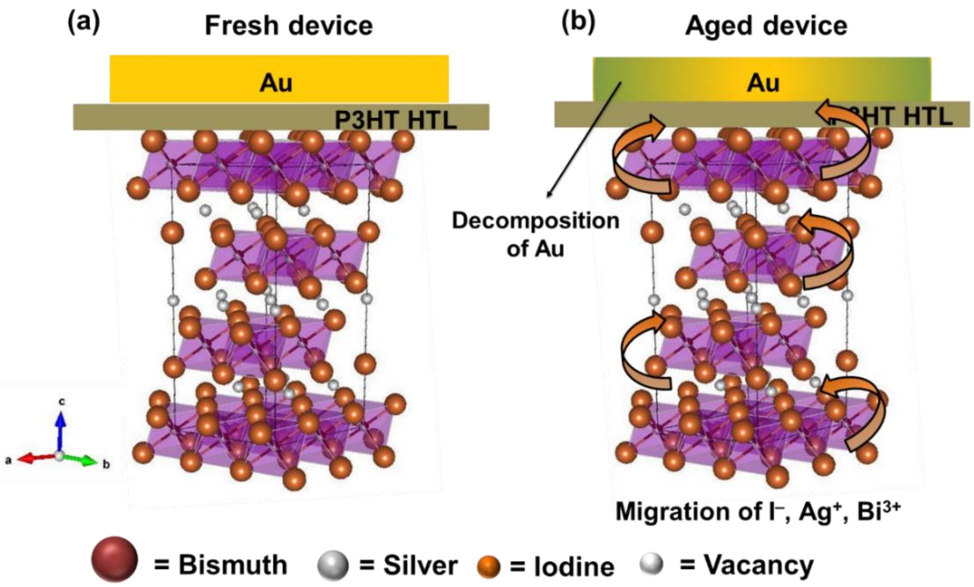

Figure 5: Schematic illustration of the proposed mechanism showing the degradation of the Ag_3BiI_6 device under an ambient atmosphere (RH = 30 – 50%).

Based on the experimental and theoretical results, a possible Ag_3BiI_6 device degradation mechanism is proposed as shown in **Figure 5**. From the theoretical studies, we observed low decomposition energy which results in degradation of Ag_3BiI_6 material to AgI and BiI_3. This corroborates with the XRD pattern where we observed residual AgI content within the Ag_3BiI_6 thin-film. Several factors can account for the migration of AgI and BiI_3 and corrosion of Au which includes the decomposition of AgI due to photochemical reaction[39] and the reaction of iodide/iodine with Au. When exposed to continuous light illumination Ag_3BiI_6 device showed linear and slow degradation (**Figure S19**) hinting towards the photochemical decomposition of residual AgI.[39] The similar and low activation energy of Ag^+ and I^- suggests fast migration of these ions. In the case of bismuth, although BiI_3 has a high migration barrier, lesser-known underpotential deposition (UPD) reaction has been reported previously showing adsorption of BiI_3 on the surface of the Au and reduction of Bi^{3+} to Bi^0 and reaction of Au with iodide/iodine.[47] The UPD adsorption reaction was also observed in Ag^+ on the surface of Au.[48] This phenomenon was also observed in lead perovskite solar cells in which Pb^{2+} in $MAPbI_3$ reduced to Pb^0 when interfaced with Au.[49] We suspect that UPD reaction might occur at the Ag_3BiI_6/P3HT (or poly(DTSTPD-*r*-BThTPD))/Au interface because of a very thin layer of HTL leading to reduction of Bi^{3+} to Bi^0 and Ag^+ to Ag^0 and corrosion of Au electrodes. However, a detailed investigation is required to validate this and is in progress. In addition, the effect of internal electric field leading to migration of Ag^+, Bi^{3+} and I^- species and corrosion of Au cannot be neglected. During the Ag_3BiI_6 crystallization, intrinsic point defects can potentially form including interstitial defects, elemental vacancy, etc.[50] In addition to these defects, voids that are observed in anti-solvent processed Ag_3BiI_6 thin-film (**Figure 1e**) become the dominant defects that facilitate the migration of ions. The previous report suggests the presence of vacancies in the Ag_3BiI_6 crystal structure.[27] Considering the vacancies, defects, interstitial sites, and voids, in addition to interstitial defects/admixtures that are present within BiI_3,[45] it is reasonable to propose vacancy mediated ion migration in Ag_3BiI_6 thin-film. The migration of Ag^+, Bi^{3+}, I^- ions near the interface with the P3HT (and poly(DTSTPD-*r*-BThTPD)) HTL promotes the diffusion of bulk elements towards the surface mainly due to the concentration gradient to achieve thermodynamic equilibrium. This further leads to the continuous loss of Bi^{3+}, Ag^+, and I^- ions from the bulk. The oxidation of Au to Au^{+1}, presence of iodine, and reduction of Ag^+ and Bi^{3+} (**Figure 4**) on the surface of Au indicate the migration and diffusion of ions through thin P3HT (and poly(DTSTPD-*r*-BThTPD)) layers and the reaction of Au with iodine to possibly form gold iodide (AuI) thereby degrading the cell. It is interesting to observe that two oppositely charged ions (i.e. Bi^{3+} and I^- or Ag^+ and I^-) accumulate at the same interface. We speculate that the reactivity of the Au electrode with volatile halide ions might partially contribute to this unusual and unique phenomenon. As we employed a thin layer of HTL, we suspect that this triple-ion migration to the electrode interface and degradation of Au can be protected by employing a thick HTL. To verify this, we initially employed thick P3HT layer by changing the spin-coating condition. To increase the thickness, the concentration of P3HT was fixed to 15 mg/mL and the spinning condition was altered. However, the PCE reduced (PCE statistics is shown in **Figure S24**) with an increase in the thickness of P3HT HTL mostly ascribing to increase in the resistance at the Ag_3BiI_6/P3HT interface. Therefore, we fabricated Ag_3BiI_6 devices with spiro-OMeTAD as HTL. We have employed spiro-OMeTAD with ethanol (EtOH) and lithium bis(trifluoromethanesulfonyl)imide (Li-TFSI) dopants[51] because the combination of widely used Li-TFSI and 4-*tert*-butylpyridine (TBP) dopants rapidly corrodes the Ag_3BiI_6 layer. The optical microscopic images showing corrosion of the Ag_3BiI_6 layer with HTL (without and with Li-TFSI and TBP dopants) are shown in **Figure S25**. After exposing the spiro-OMeTAD HTL based device to the ambient atmosphere, no visible change in the color of the Au electrode was observed and the device showed stable efficiency, as shown in **Figure S26b**, suggesting the suppression of ion migration. The J-V curve of the Ag_3BiI_6 device employing spiro-OMeTAD is shown in **Figure S26a**. Based on our present results, we presume that suppressing residual AgI content might help to avoid Ag_3BiI_6 material and device degradation. Phase pure Ag_3BiI_6 without residual AgI might be obtained by exploring suitable solvents and/or additives. Efforts to replace the Au metal electrode with a more stable and inert electrode can also be a significant step in enhancing the stability. Despite the antagonistic influence on photovoltaic device stability, the migration of ions in Ag_3BiI_6 can allow its extensive application in photodetectors[52] (to facilitate fast response) and in resistive-switching memory devices.[53]

CONCLUSION

In conclusion, this work reported efficient solar cells based on $AgBi_2I_7$, Ag_2BiI_5, and Ag_3BiI_6 light absorbers. The long-term stability of devices under ambient humidity atmosphere reveals that Ag_3BiI_6 adopts unique triple-ion migration where Ag^+, Bi^{3+}, and I^- ions migrate and diffuse through hole-transport layer (HTL) contrasting the case of Ag_2BiI_5 and $AgBi_2I_7$. The theoretical study suggests low decomposition enthalpy favors the decomposition of Ag_3BiI_6 to AgI and BiI_3 causing migration and diffusion of ions. This migration is more pronounced in anti-solvent-processed Ag_3BiI_6 thin-film-based devices as it showed faster degradation in the device performance compared to without anti-solvent one and was relieved by using a thick HTL in solar cells. The unusual triple-ion-migration behavior in Ag_3BiI_6 accentuates the importance of not only understanding and improving the Ag_3BiI_6 material for better solar cell design but also stimulate the use of this unique behavior in other optoelectronics such as photodetector and switching memory devices.

ACKNOWLEDGEMENTS

The present research has been supported by the Japanese Society for Promotion of Science (JSPS) with Grant-in-Aid for Scientific Research S as well as for International Fellowships for Research Program. Ashish Kulkarni thanks funding support from the Japan Society for Promotion of Sciences (JSPS) postdoctoral (PD) fellowship. Feray Ünlü and Sanjay Mathur gratefully acknowledge the University of Cologne (Excellence Program "Quantum Matter and Materials") and the German Science Foundation (DFG) for the funding provided in the framework of the Priority Programm SPP2196. The authors thank DAAD for a bilateral mobility grant supporting the exchange visit of researchers between the University of Cologne, Germany, and the RMIT

University, Melbourne, Australia (Project-ID 57388639). The authors acknowledge Hanming Liu, Daniele Cuzzupe, and Khan Lê for PL measurements. The authors acknowledge Mitsubishi Chemical Cooperation for their support in providing poly(DTSTPD-*r*-BThTPD) hole transport layer. The authors acknowledge Professor H. Segawa for providing access to research facilities at Research Center for Advanced Science and Technology (RCAST), The University of Tokyo.

Dedication

Dedicated to Anil Madhavrao Deshpande (Kaka Saheb) and others who lost their life due to COVID-19.

REFERENCES

[1] Akihiro Kojima, K. Teshima, Y. Shirai, T. Miyasaka, *J. Am. Chem. Soc.* **2009**, *131*, 6050–6051.

[2] A. K. Jena, A. Kulkarni, T. Miyasaka, *Chem. Rev.* **2019**, *119*, 3036–3103.

[3] NREL, “Best Research-Cell Efficiency Chart,” can be found under https://www.nrel.gov/pv/cell-efficiency.html, **2021**.

[4] T. Miyasaka, A. Kulkarni, G. M. Kim, S. Öz, A. K. Jena, *Adv. Energy Mater.* **2020**, *10*, 1902500.

[5] M. H. Futscher, J. M. Lee, L. McGovern, L. A. Muscarella, T. Wang, M. I. Haider, A. Fakharuddin, L. Schmidt-Mende, B. Ehrler, *Mater. Horizons* **2019**, *6*, 1497–1503.

[6] N. Liu, C. Yam, *Phys. Chem. Chem. Phys.* **2018**, *20*, 6800–6804.

[7] S. Öz, A. K. Jena, A. Kulkarni, K. Mouri, T. Yokoyama, I. Takei, F. Ünlü, S. Mathur, T. Miyasaka, *ACS Energy Lett.* **2020**, *5*, 1292–1299.

[8] N. Pant, A. Kulkarni, M. Yanagida, Y. Shirai, T. Miyasaka, K. Miyano, *Adv. Mater. Interfaces* **2020**, *7*, 1901748.

[9] A. Babayigit, A. Ethirajan, M. Muller, B. Conings, *Nat. Mater.* **2016**, *15*, 247–251.

[10] S. Gu, R. Lin, Q. Han, Y. Gao, H. Tan, J. Zhu, *Adv. Mater.* **2020**, *32*, 1907392.

[11] Z. Jin, Z. Zhang, J. Xiu, H. Song, T. Gatti, Z. He, *J. Mater. Chem. A* **2020**, *8*, 16166–16188.

[12] B. Ghosh, S. Chakraborty, H. Wei, C. Guet, S. Li, S. Mhaisalkar, N. Mathews, *J. Phys. Chem. C* **2017**, *121*, 17062–17067.

[13] B. Ghosh, B. Wu, H. K. Mulmudi, C. Guet, K. Weber, T. C. Sum, S. Mhaisalkar, N. Mathews, *ACS Appl. Mater. Interfaces* **2018**, *10*, 35000–35007.

[14] A. Kulkarni, T. Singh, M. Ikegami, T. Miyasaka, *RSC Adv.* **2017**, *7*, 9456–9460.

[15] B. W. Park, B. Philippe, X. Zhang, H. Rensmo, G. Boschloo, E. M. J. Johansson, *Adv. Mater.* **2015**, *27*, 6806–6813.

[16] Y. Kim, Z. Yang, A. Jain, O. Voznyy, G. H. Kim, M. Liu, L. N. Quan, F. P. García de Arquer, R. Comin, J. Z. Fan, E. H. Sargent, *Angew. Chemie - Int. Ed.* **2016**, *55*, 9586–9590.

[17] A. Kulkarni, A. K. Jena, M. Ikegami, T. Miyasaka, *Chem. Commun.* **2019**, 5–8.

[18] H. Zhu, M. Pan, M. B. Johansson, E. M. J. J. Johansson, *ChemSusChem* **2017**, *10*, 2592–2596.

[19] I. Turkevych, S. Kazaoui, E. Ito, T. Urano, K. Yamada, H. Tomiyasu, H. Yamagishi, M. Kondo, S. Aramaki, *ChemSusChem* **2017**, *10*, 3754–3759.

[20] N. Pai, J. Lu, T. R. Gengenbach, A. Seeber, A. S. R. Chesman, L. Jiang, D. C. Senevirathna, P. C. Andrews, U. Bach, Y.-B. Cheng, A. N. Simonov, *Adv. Energy Mater.* **2018**, 1803396.

[21] Y. Seo, S. R. Ha, S. Yoon, S. M. Jeong, H. Choi, D.-W. Kang, *J. Power Sources* **2020**, *453*, 227903.

[22] A. K. Baranwal, H. Masutani, H. Sugita, H. Kanda, S. Kanaya, N. Shibayama, Y. Sanehira, M. Ikegami, Y. Numata, K. Yamada, T. Miyasaka, T. Umeyama, H. Imahori, S. Ito, *Nano Converg.* **2017**, *4*.

[23] H.-W. Chen, N. Sakai, M. Ikegami, T. Miyasaka, *J. Phys. Chem. Lett.* **2015**, *6*, 164–169.

[24] H. J. Snaith, A. Abate, J. M. Ball, G. E. Eperon, T. Leijtens, N. K. Noel, S. D. Stranks, J. T. W. Wang, K. Wojciechowski, W. Zhang, *J. Phys. Chem. Lett.* **2014**, *5*, 1511–1515.

[25] A. K. Jena, A. Kulkarni, M. Ikegami, T. Miyasaka, *J. Power Sources* **2016**, *309*, 1–10.

[26] Y. Yuan, Q. Wang, J. Huang, in *Org. Halide Perovskite Photovoltaics From Fundam. to Device Archit.* (Eds.: N.G. Park, M. Grätzel, T. Miyasaka), Springer, **2016**, pp. 137–162.

[27] T. Oldag, T. Aussieker, H. L. Keller, C. Preitschaft, A. Pfitzner, *Zeitschrift fur Anorg. und Allg. Chemie* **2005**, *631*, 677–682.

[28] J. L. Minns, P. Zajdel, D. Chernyshov, W. van Beek, M. A. Green, *Nat. Commun.* **2017**, *8*, 15152.

[29] C. Besleaga, L. E. Abramiuc, V. Stancu, A. G. Tomulescu, M. Sima, L. Trinca, N. Plugaru, L. Pintilie, G. A. Nemnes, M. Iliescu, H. G. Svavarsson, A. Manolescu, I. Pintilie, *J. Phys. Chem. Lett.* **2016**, *7*, 5168–5175.

[30] A. Koedtruad, M. Goto, M. Amano Patino, Z. Tan, H. Guo, T. Nakamura, T. Handa, W. T. Chen, Y. C. Chuang, H. S. Sheu, T. Saito, D. Kan, Y. Kanemitsu, A. Wakamiya, Y. Shimakawa, *J. Mater. Chem. A* **2019**, *7*, 5583–5588.

[31] L. F. Mashadieva, Z. S. Aliev, A. V. Shevelkov, M. B. Babanly, *J. Alloys Compd.* **2013**, *551*, 512–520.

[32] B. Ghosh, B. Wu, X. Guo, P. C. Harikesh, R. A. John, T. Baikie, Arramel, A. T. S. Wee, C. Guet, T. C. Sum, S. Mhaisalkar, N. Mathews, *Adv. Energy Mater.* **2018**, *8*, 1802051.

[33] Y. Bekenstein, J. C. Dahl, J. Huang, W. T. Osowiecki, J. K. Swabeck, E. M. Chan, P. Yang, A. P. Alivisatos, *Nano Lett.* **2018**, *18*, 3502–3508.

[34] S. Svanström, T. J. Jacobsson, G. Boschloo, E. M. J. Johansson, H. Rensmo, U. B. Cappel, *ACS Appl. Mater. Interfaces* **2020**, *12*, 7212–7221.

[35] A. Crovetto, A. Hajijafarassar, O. Hansen, B. Seger, I. Chorkendorff, P. C. K. Vesborg, *Chem. Mater.* **2020**, *32*, 3385–3395.

[36] N. Pant, A. Kulkarni, M. Yanagida, Y. Shirai, T. Miyasaka, K. Miyano, *ACS Appl. Energy Mater.* **2020**, *3*, 6215–6221.

[37] T. Kirchartz, J. A. Márquez, M. Stolterfoht, T. Unold, *Adv. Energy Mater.* **2020**, *10*, DOI 10.1002/aenm.201904134.

[38] Z. Guo, A. K. Jena, I. Takei, G. M. Kim, M. A. Kamarudin, Y. Sanehira, A. Ishii, Y. Numata, S. Hayase, T. Miyasaka, *J. Am. Chem. Soc.* **2020**, *142*, 9725–9734.

[39] E. J. Hartung, *J. Chem. Soc.* **1926**, *129*, 1349–1354.

[40] J. F. Moulder, J. Chastain, *Handbook of X-Ray Photoelectron Spectroscopy: A Reference Book of Standard Spectra for Identification and Interpretation of XPS Data*, Physical Electronics Division, Perkin-Elmer Corporation, **1992**.

[41] K. Kwon, B. L. Suh, K. Park, J. Kim, H.-T. Jung, *Sci. Rep.* **2019**, *9*, 3885.

[42] M. P. Casaletto, A. Longo, A. Martorana, A. Prestianni, A. M. Venezia, *Surf. Interface Anal.* **2006**, *38*, 215–218.

[43] Y. Kato, L. K. Ono, M. V Lee, S. Wang, S. R. Raga, Y. Qi, *Adv. Mater. Interfaces* **2015**, *2*, 1500195.

[44] W. E. Morgan, W. J. Stec, J. R. Van Wazer, *Inorg. Chem.* **1973**, *12*, 953–955.

[45] A. Kulkarni, T. Singh, A. K. Jena, P. Pinpithak, M. Ikegami, T. Miyasaka, *ACS Appl. Mater. Interfaces* **2018**, *10*, 9547–9554.

[46] W. Czaja, G. Harbeke, L. Krausbauer, E. Meier, B. J. Curtis, H. Brunner, E. Tosatti, *Solid State Commun.* **1973**, *13*, 1445–1449.

[47] Y.-L. Du, C.-M. Wang, *Chinese J. Chem.* **2002**, *20*, 596–600.

[48] E. Herrero, L. J. Buller, H. D. Abruña, *Chem. Rev.* **2001**, *101*, 1897–1930.

[49] R. A. Kerner, P. Schulz, J. A. Christians, S. P. Dunfield, G. Teeter, J. J. Berry, B. P. Rand, *APL Mater.* **2019**, *7*, 041103.

[50] L. Liang, P. Gao, *Adv. Sci.* **2018**, *5*, 1700331.

[51] Z. Hu, Z. Wang, G. Kapil, T. Ma, S. Iikubo, T. Minemoto, K. Yoshino, T. Toyoda, Q. Shen, S. Hayase, *ChemSusChem* **2018**, *11*, 2930–2935.

[52] H. Wang, M. Zhou, H. Luo, *ACS Omega* **2018**, *3*, 1445–1450.

[53] X. Guan, W. Hu, M. A. Haque, N. Wei, Z. Liu, A. Chen, T. Wu, *Adv. Funct. Mater.* **2018**, *28*, 1704665.